

Supporting Information

In-situ grown MnO₂/Graphdiyne oxide hybrid 3D nanoflowers for high performance aqueous zinc-ion batteries

Fuhui Wang,^{a, b} Weiyue Jin,^{a, b} Zecheng Xiong,^{a, b} Huibiao Liu^{✉a, b}

^a *Beijing National Laboratory for Molecular Sciences, CAS Research/Education Center for Excellence in Molecular Sciences, CAS Key Laboratory of Organic Solids, Institute of Chemistry, Chinese Academy of Sciences, Beijing 100190, P. R. China.*

^b *University of Chinese Academy of Sciences, Beijing 100049, P. R. China*

E-mail: liuhb@iccas.ac.cn

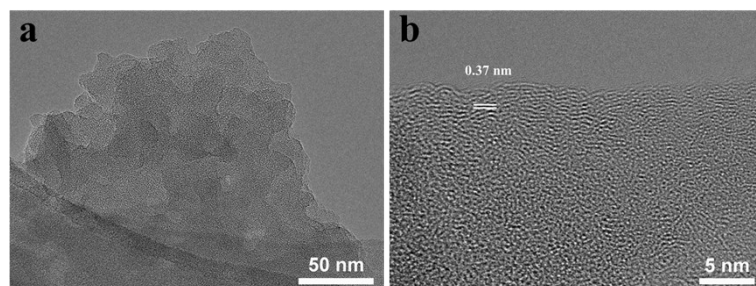


Fig. S1 (a) TEM and (b) HR-TEM images of GDYO nanosheet.

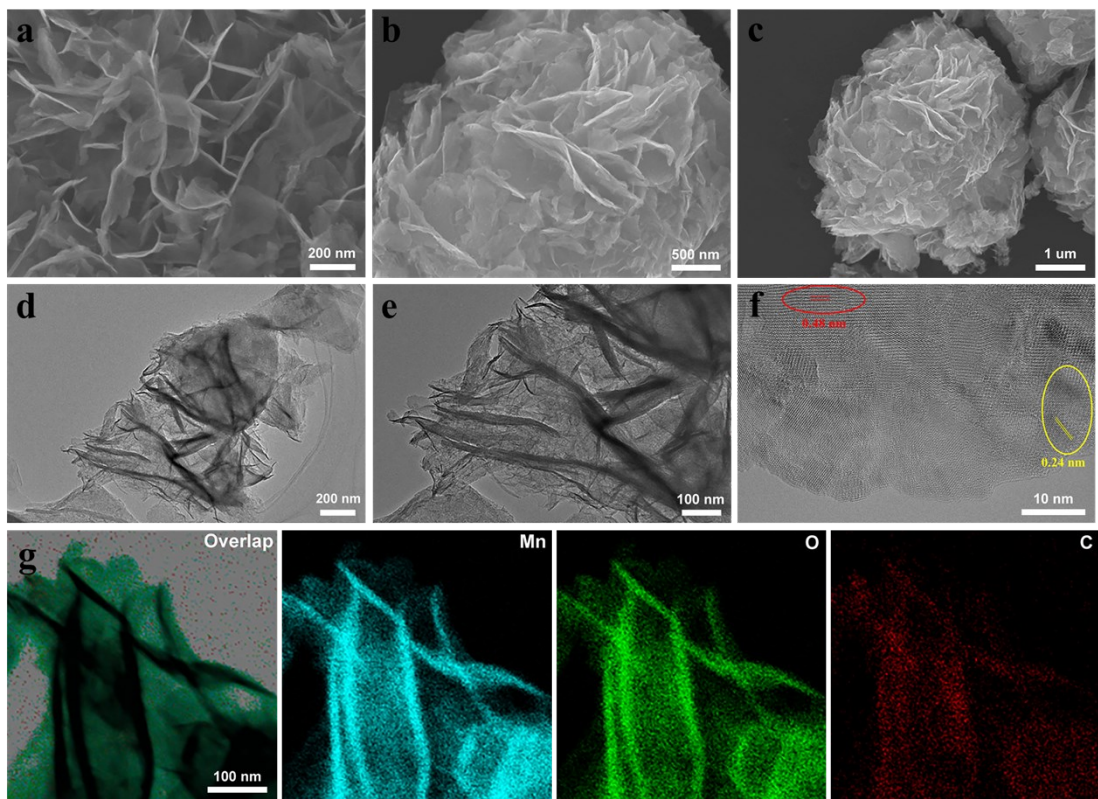


Fig. S2 Microstructural and compositional analysis of $\text{MnO}_2@10\text{GDYO}$ hybrid 3D nanoflowers.
(a-c) SEM images. (d-e) TEM images. (f) HR-TEM image and (g) elemental mapping images of Mn, O and C.

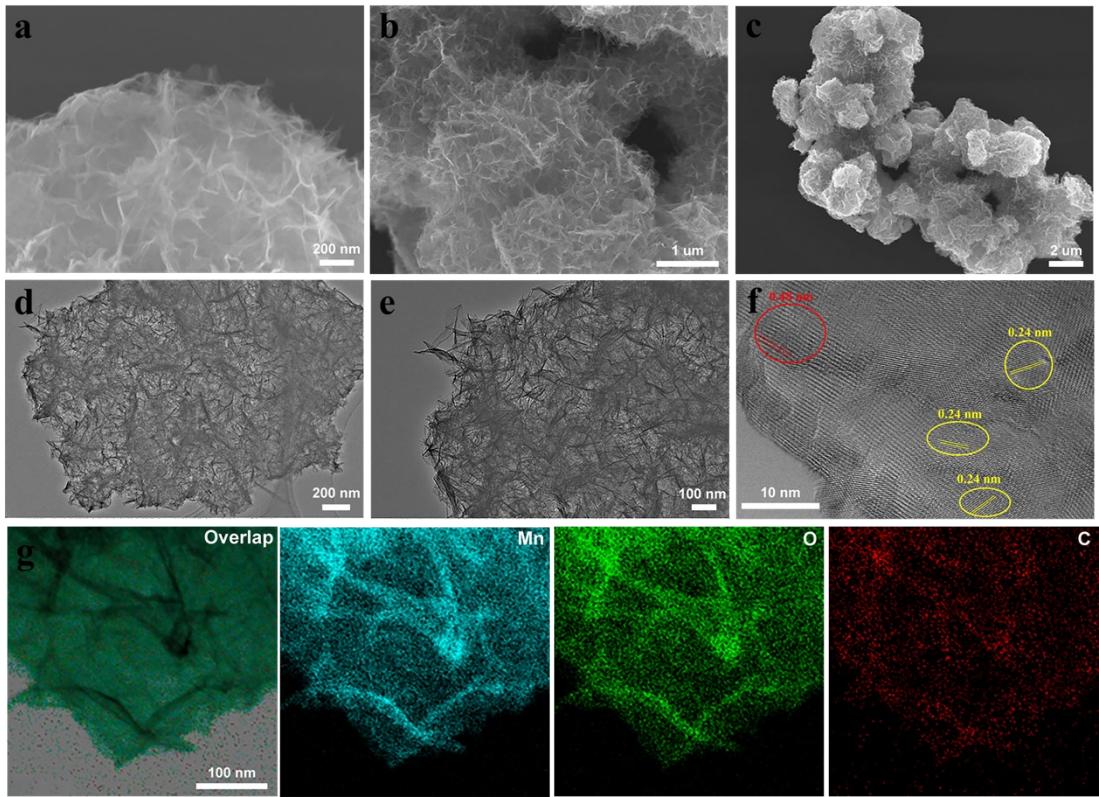


Fig. S3 Microstructural and compositional analysis of $\text{MnO}_2@20\text{GDYO}$ hybrid 3D nanoflowers.
(a-c) SEM images. (d-e) TEM images. (f) HR-TEM image and (g) elemental mapping images of Mn, O and C.

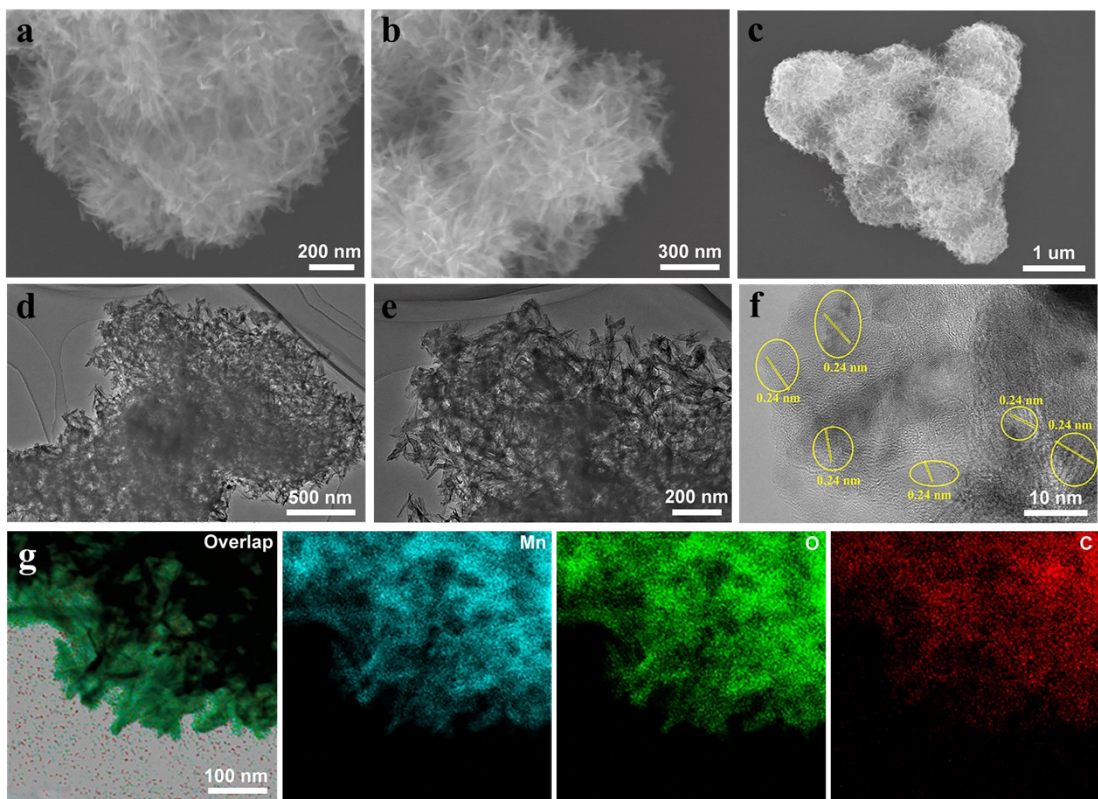


Fig. S4 Microstructural and compositional analysis of MnO_2 @100GDYO hybrid 3D nanoflowers. (a-c) SEM images. (d-e) TEM images. (f) HR-TEM image and (g) elemental mapping images of Mn, O and C.

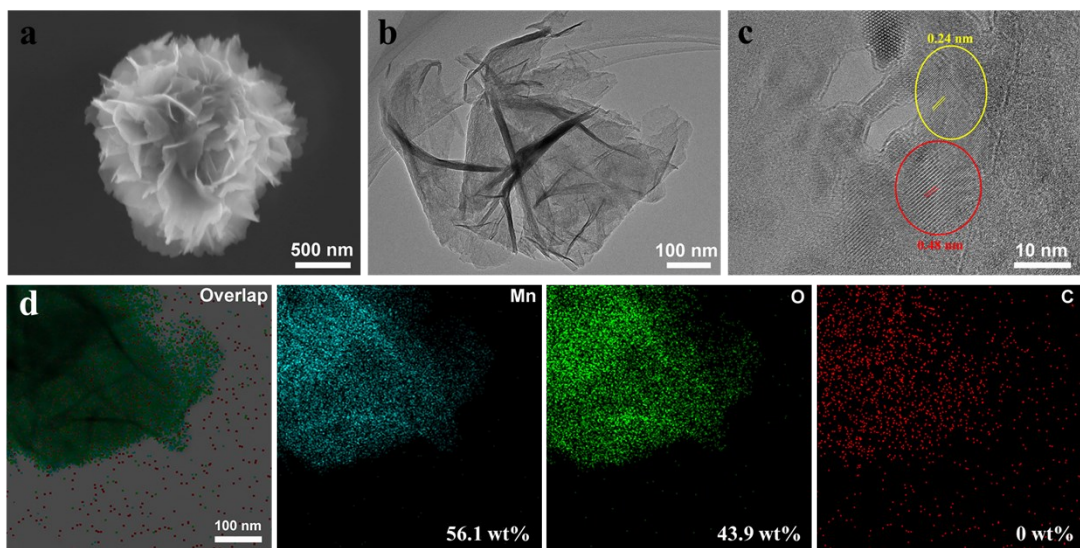


Fig. S5 Microstructural and compositional analysis of MnO_2 . (a) SEM image. (b) TEM image. (c) HR-TEM image and (d) elemental mapping images of Mn, O and C.

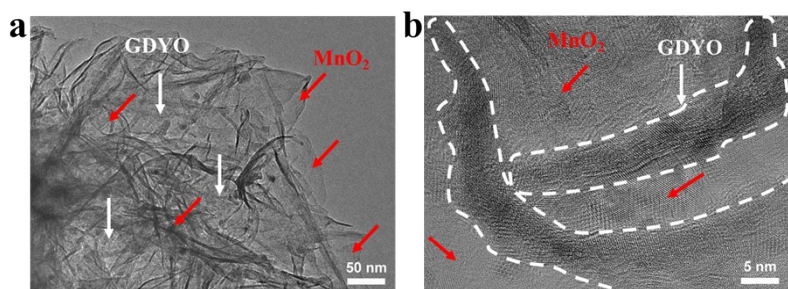


Fig. S6 (a) TEM and (b) HR-TEM images of MnO₂@50GDYO hybrid 3D nanoflowers.

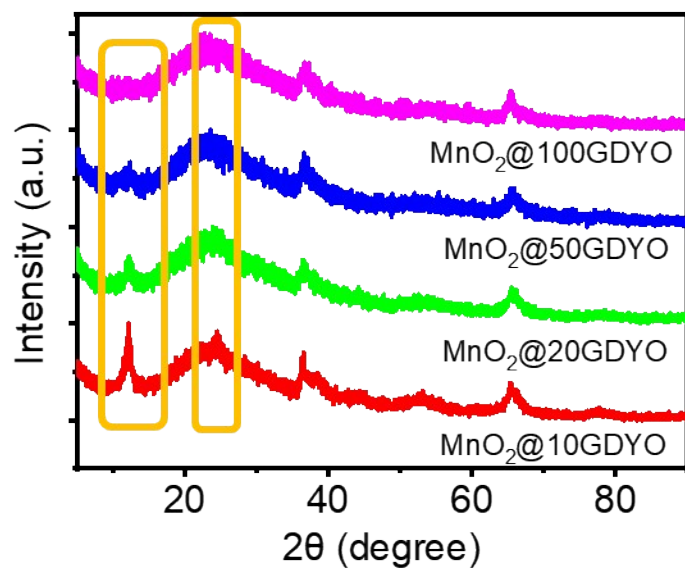


Fig. S7 XRD patterns of MnO₂@GDYO hybrid 3D nanoflowers.

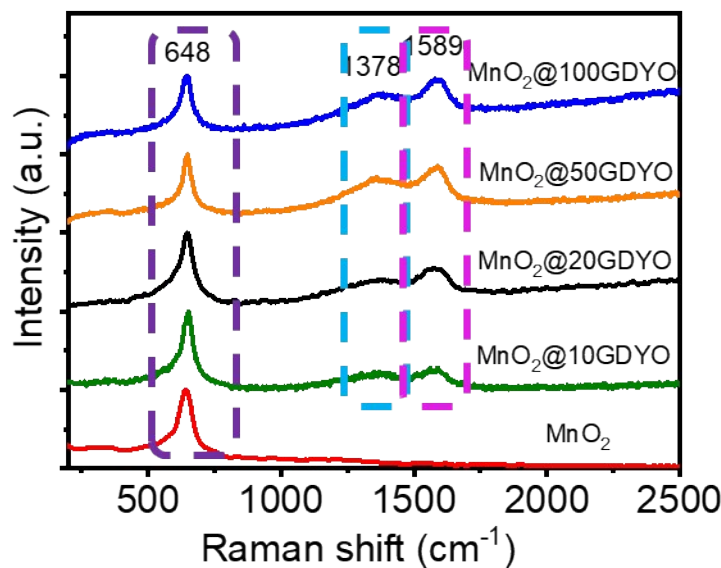


Fig. S8 Raman spectra of MnO_2 and $\text{MnO}_2@\text{GDYO}$ hybrid 3D nanoflowers.

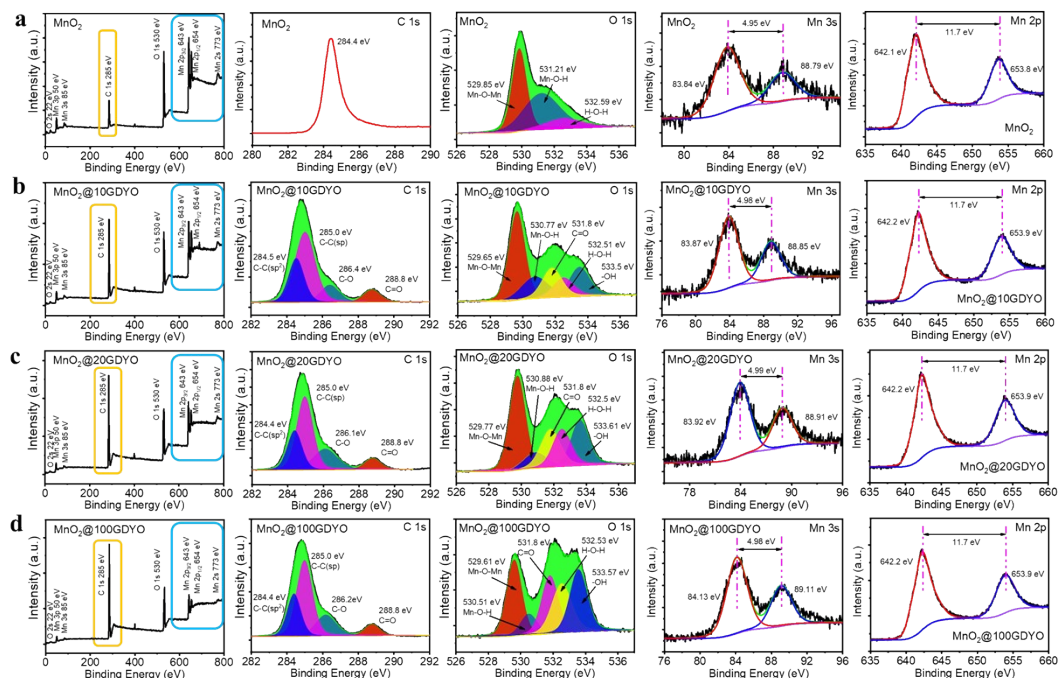


Fig. S9 XPS spectra of MnO_2 and $\text{MnO}_2@\text{GDYO}$ hybrid 3D nanoflowers. (a-d) Survey scan and narrow scan for element C, O, Mn.

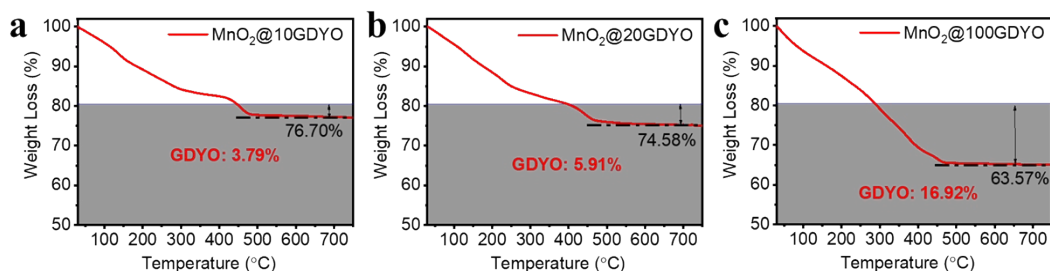


Fig. S10 TGA curves of (a) $\text{MnO}_2@\text{10GDYO}$, (b) $\text{MnO}_2@\text{20GDYO}$ and (c) $\text{MnO}_2@\text{100GDYO}$ hybrid 3D nanoflowers.

Tab. S1 Comparison of specific surface area of MnO_2 with different synthetic methods and morphologies

Materials	Preparation	Morphology	Specific surface area ($\text{m}^2 \text{ g}^{-1}$)	Ref.
MnO_2	solvothermal	nanowires	81.9	1
N-CNSs@ MnO_2	hydrothermal	nanoflakes	7.3	2
MnO_2 -	mechanical	nanosheets	99.04	3
CNTs/CNHs	mixing			
MnO_2/rGO	vacuum filtration	nanowires	159.9	4
$\alpha\text{-MnO}_2/\text{CNT}$	chemical precipitation	microspheres	119.3	5
HMs				
MnO_2	chemical precipitation	nanospheres	178	6
$\beta\text{-MnO}_2$	microwave hydrothermal	nanofibers	□68	7
Graphene- MnO_2	hydrothermal	nanotube	136.2	8
$\text{MnO}_2@\text{50GDYO}$	in-situ induced	3D nanoflowers	204.83	This work

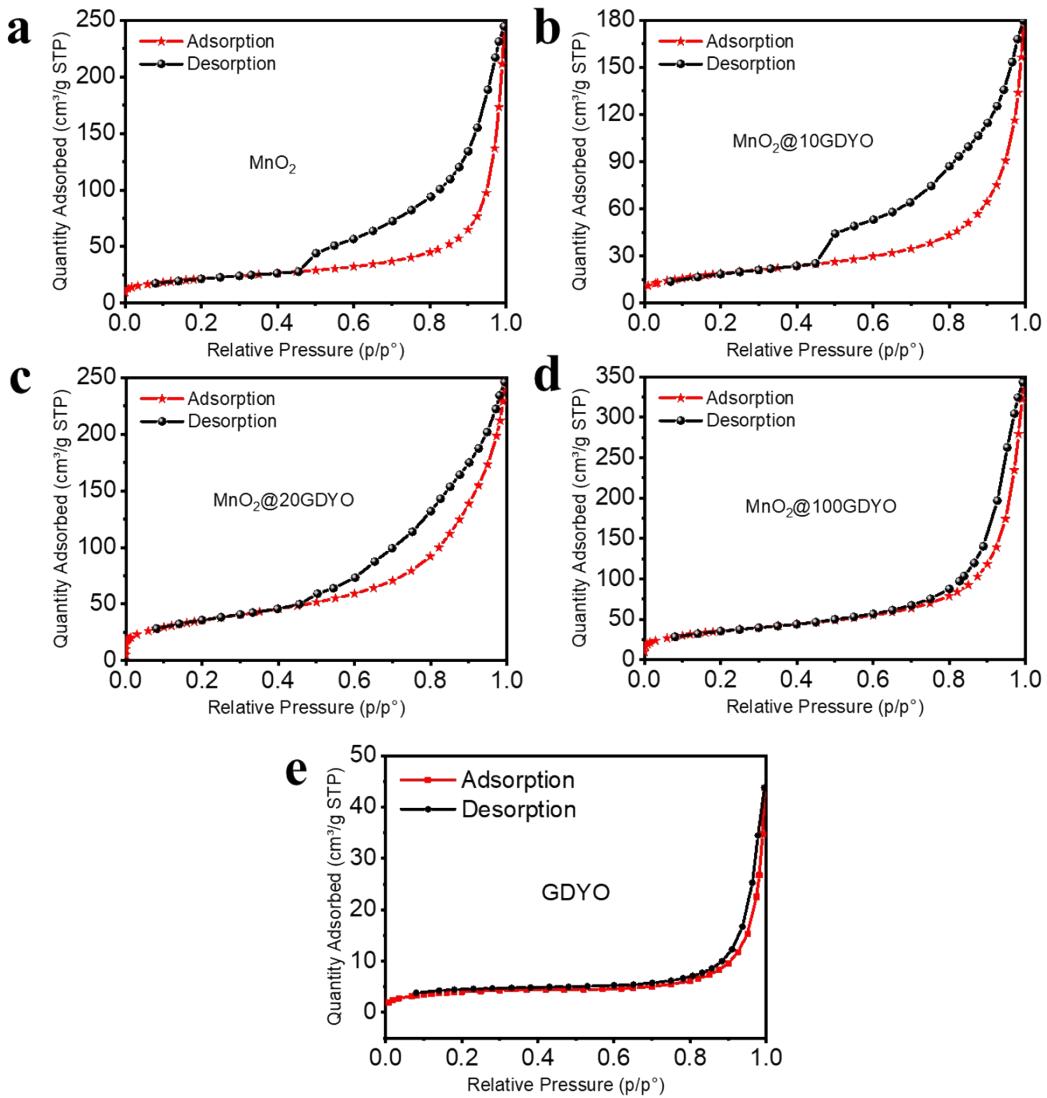


Fig. S11 Nitrogen adsorption-desorption isotherms of (a) MnO_2 , (b) $\text{MnO}_2@10\text{GDYO}$, (c) $\text{MnO}_2@20\text{GDYO}$, (d) $\text{MnO}_2@100\text{GDYO}$ hybrid 3D nanoflowers and (e) GDYO at 77 K.

The BET specific surface area of GDYO is $14.7253 \text{ m}^2 \text{ g}^{-1}$, according to the Nitrogen adsorption-desorption isotherm.

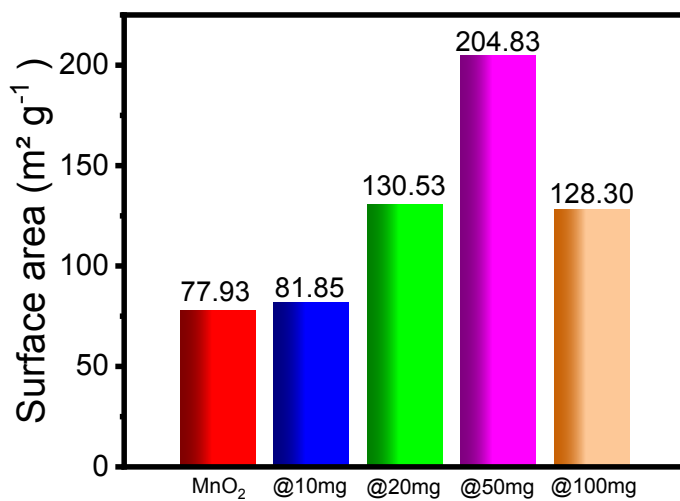


Fig. S12 Specific surface area of MnO₂ and MnO₂@GDYO hybrid 3D nanoflowers.

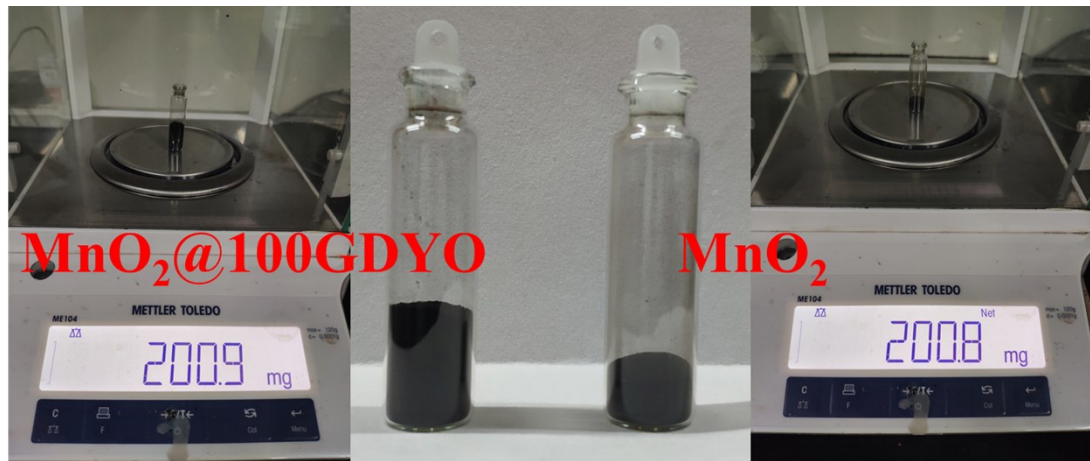


Fig. S13 Photographs of MnO₂ and MnO₂@100GDYO samples with approximate weight.

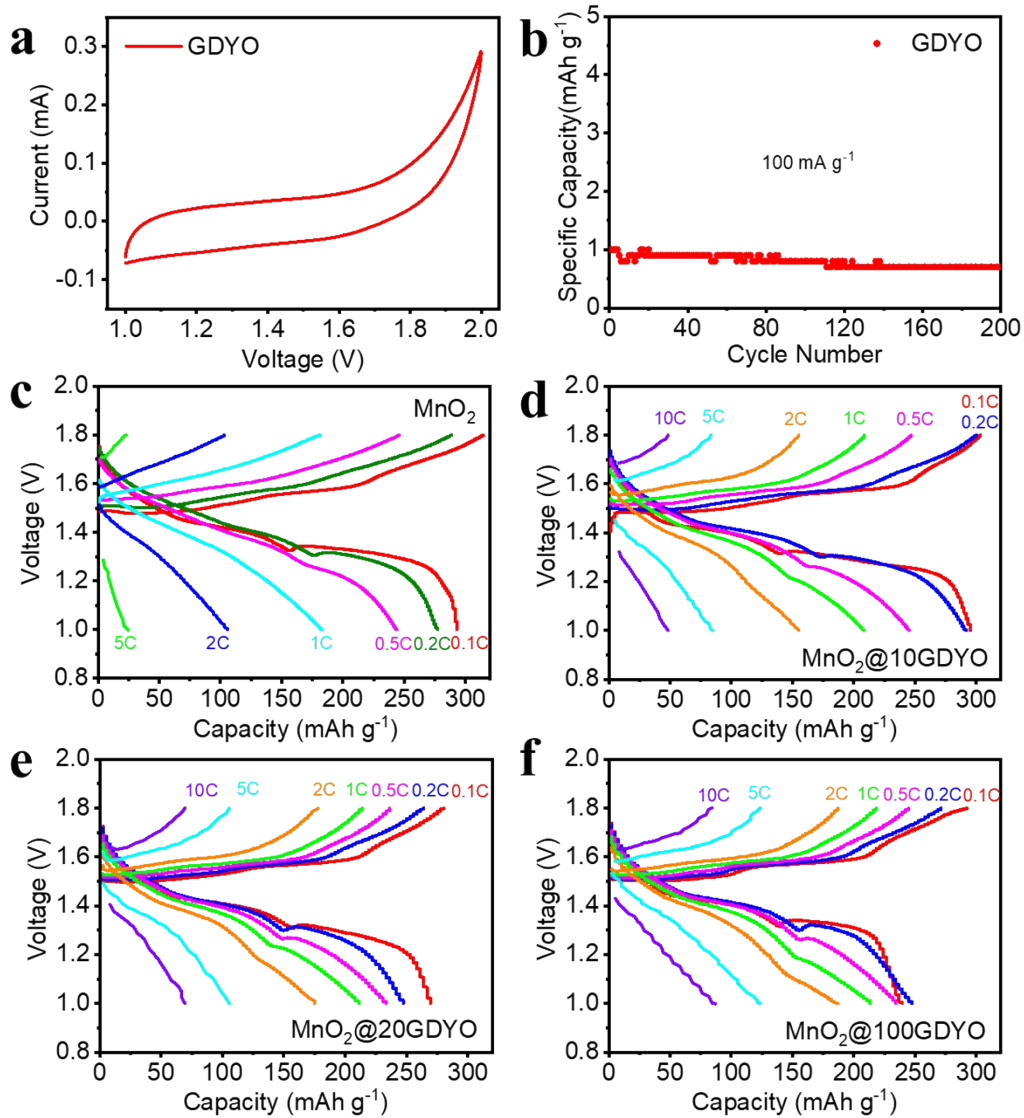


Fig. S14 (a) CV curves of GDYO at 0.1 mV s^{-1} . (b) Cycle performances of GDYO at 100 mA h g^{-1} . Charge and discharge curves of (c) MnO_2 , (d) $\text{MnO}_2@10\text{GDYO}$, (e) $\text{MnO}_2@20\text{GDYO}$ and (f) $\text{MnO}_2@100\text{GDYO}$ electrodes at current densities ranging from 0.1 to 10 C.

It can be seen from the CV curve of GDYO that there is no redox peak in the voltage range of 1 - 2V, and the current increase when the voltage is greater than 1.8V is caused by the decomposition of the electrolyte. The specific capacity of GDYO tested at current density of 100 mA g^{-1} is approximately 1 mA h g^{-1} , which is negligible. Therefore, it is concluded that the GDYO has no capacity contribution to zinc ion storage.

Tab. S2 Comparison of reported MnO_2 cathode materials for Zn-ion batteries

Materials	Low-rate capacity (mA h g⁻¹)	High-rate capacity (mA h g⁻¹)	Capacity retention	Cycling stability	Ref.
Graphene-MnO ₂	321 (48 mA g ⁻¹)	147 (1200 mA g ⁻¹)	45.8%	91% after 300 cycles at 720 mA g ⁻¹	8
N-CNSs@MnO ₂	303.7 (0.2 A g ⁻¹)	114.3 (10 A g ⁻¹)	37.6%	81.2% after 200 cycles at 8 A g ⁻¹	2
MnO ₂	171 (1 C)	87 (30 C)	50.9%	□ 30% after 1000 cycles at 20 C	9
MnO ₂ -rGO	275 (0.3 A g ⁻¹)	180 (3 A g ⁻¹)	65.5%	□ 74.3% after 500 cycles at 3 A g ⁻¹	3
MnO ₂	200 (0.3 A g ⁻¹)	60 (3 A g ⁻¹)	30%	500 cycles at 0.6 A g ⁻¹	1
MnO ₂ /rGO	317 (0.1 A g ⁻¹)	112 (7.5 A g ⁻¹)	35.33%	76.2% after 600 cycles at 1 A g ⁻¹	4
MnO ₂	264 (0.2 C)	58 (3 C)	21.97%	99.4% after 1000 cycles at 1 C	10
K _{0.28} MnO ₂	238 (0.1 A g ⁻¹)	83 (5 A g ⁻¹)	35%	95% after 1000 cycles at 2 A g ⁻¹	11
α-MnO ₂ -C-30	298.2 (0.1 A g ⁻¹)	170 (2 A g ⁻¹)	57%	□ 33% after 100 cycles at 0.5 A g ⁻¹	12
MnO ₂ @50GDYO 3D nanoflowers	265.1 (0.1 C)	80.6 (10 C)	30.4%	77.6% after 1000 cycles at 5 C	This work

1 C = 308 mA h g⁻¹

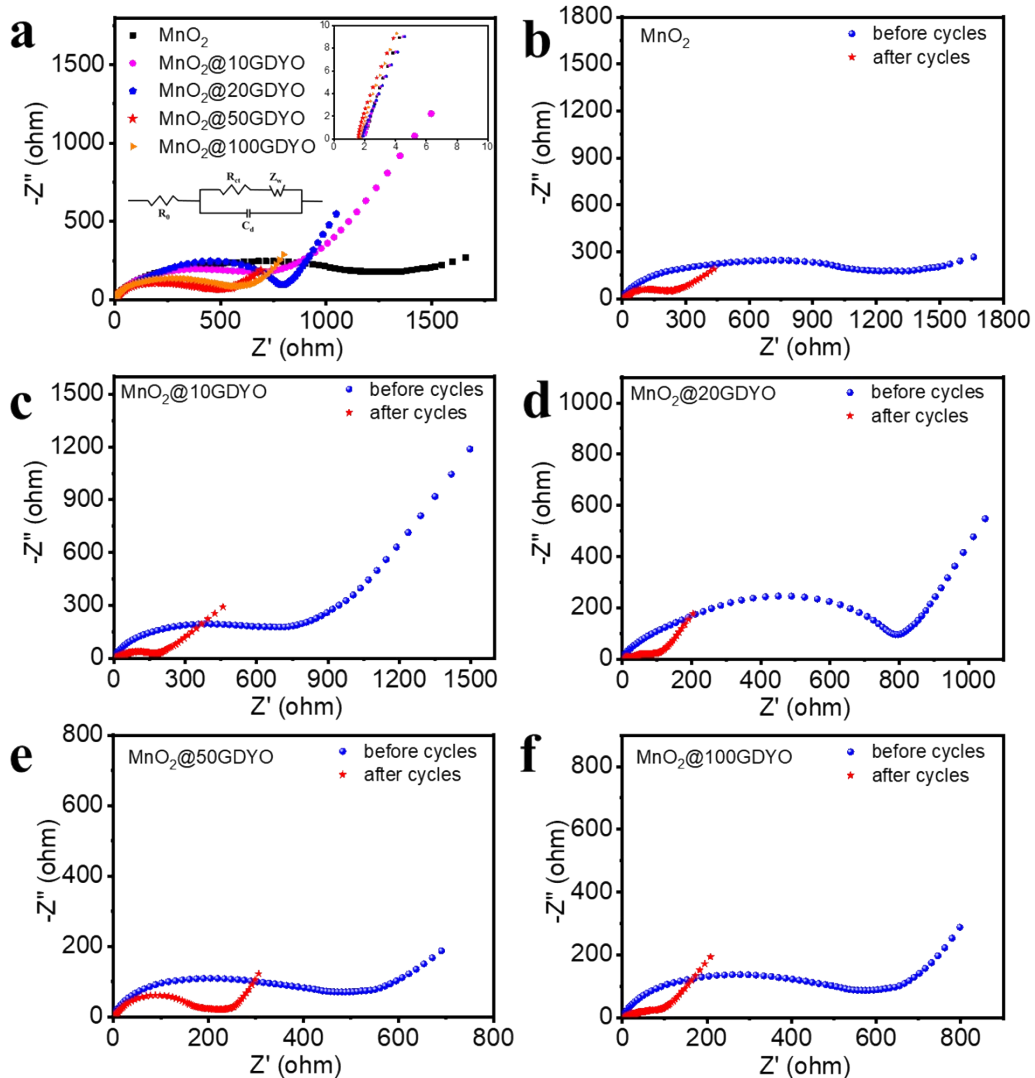


Fig. S15 Nyquist plots of the impedance spectra of MnO_2 and $\text{MnO}_2@\text{GDYO}$ electrodes before and after cycles.

Tab. S3 Fitting results of R_0 , R_{ct} of the EIS based on the equivalent circuit.

Materials	R_0 (Ω)	R_{ct} (Ω)
MnO_2	2.23	1265
$\text{MnO}_2@10\text{GDYO}$	2.07	836
$\text{MnO}_2@20\text{GDYO}$	1.98	790
$\text{MnO}_2@50\text{GDYO}$	1.76	513
$\text{MnO}_2@100\text{GDYO}$	1.88	612

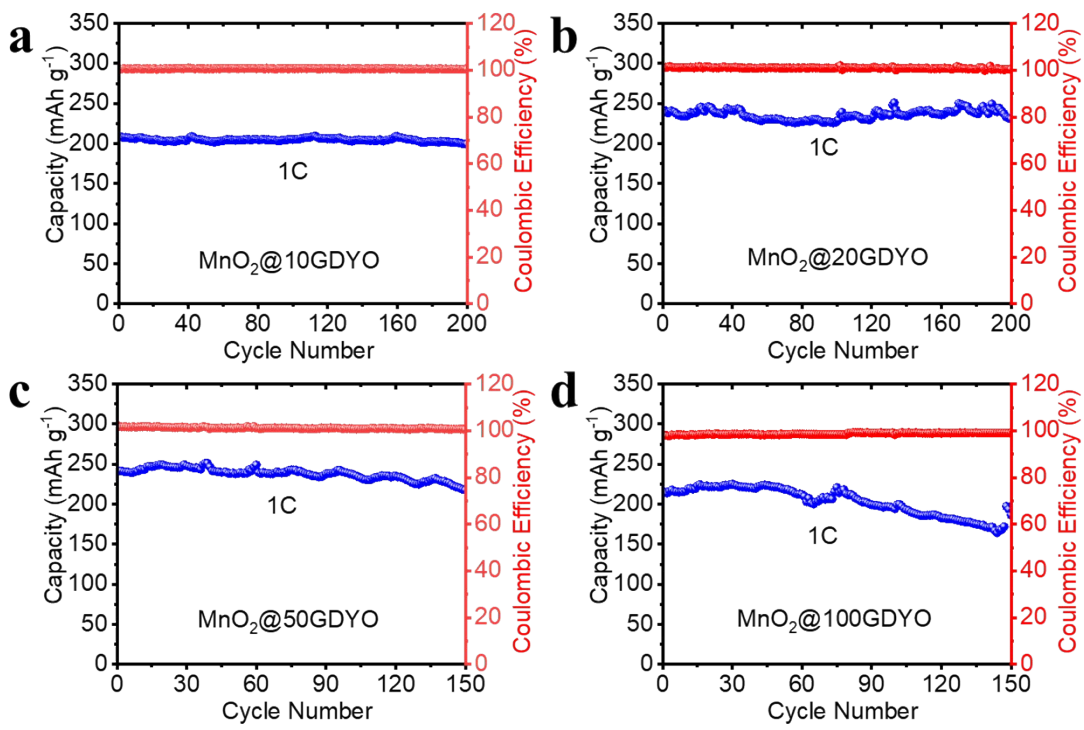


Fig. S16 Long-term cycling performance of (a) MnO₂@10GDYO, (b) MnO₂@20GDYO and (c) MnO₂@100GDYO electrodes at 1 C after rate performances test.

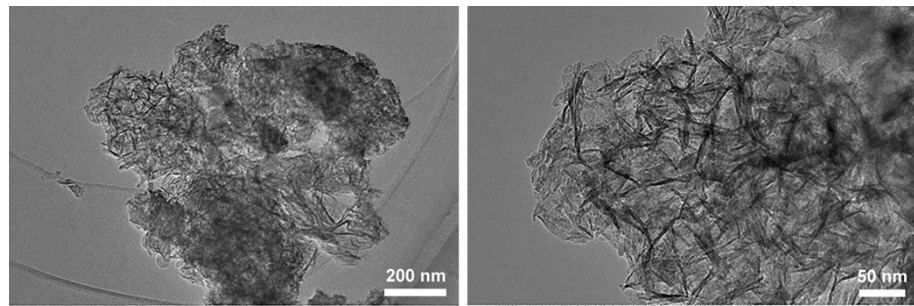


Fig. S17 TEM images of the MnO₂@50GDYO hybrid 3D nanoflowers after discharge-charge test.

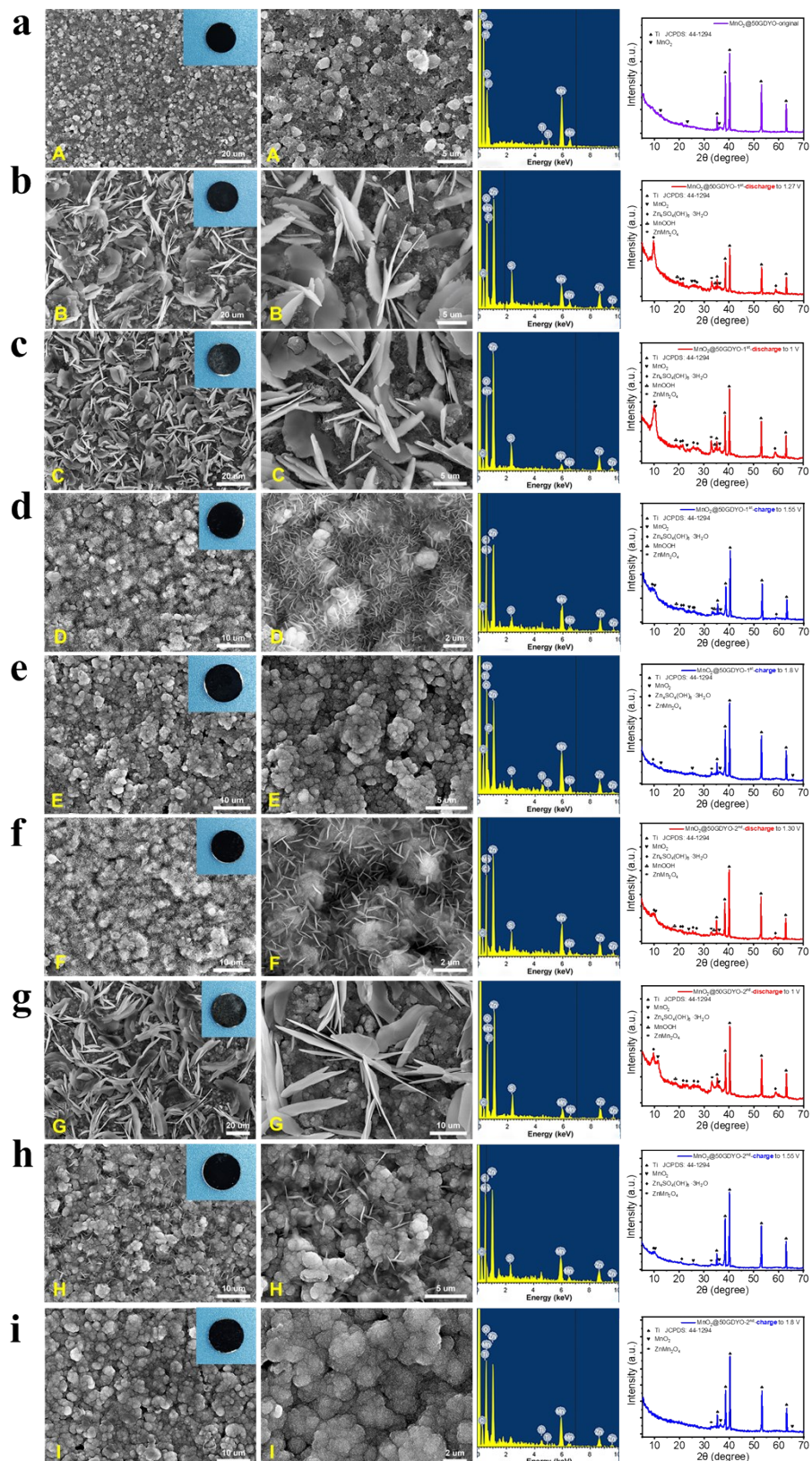


Fig. S18 Photographs, SEM images and their corresponding elemental mapping, XRD patterns at various states marked in Fig. 5a.

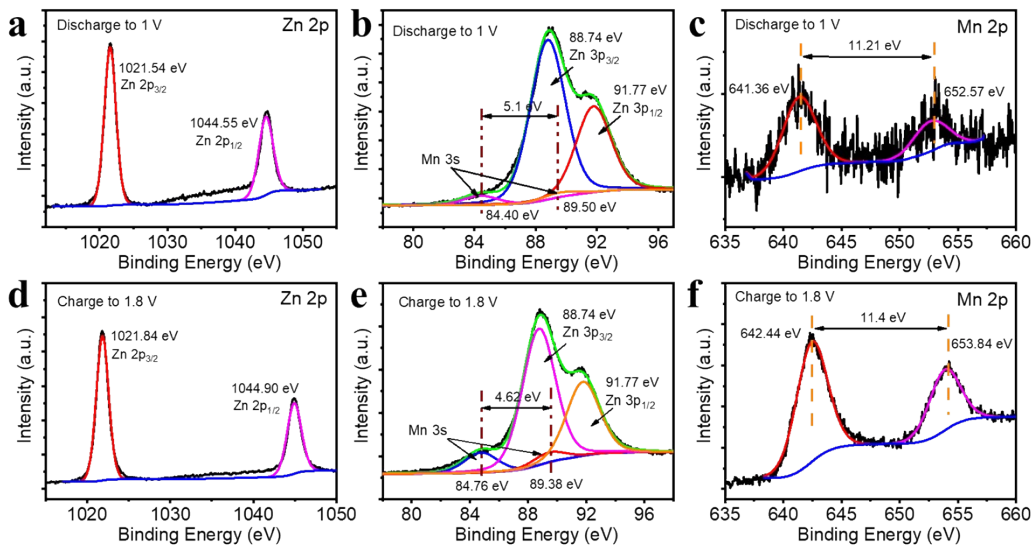


Fig. S19 XPS narrow scan spectra for element Zn and Mn of $\text{MnO}_2@50\text{GDYO}$ electrodes at full discharge and charge state.

With deep discharging to 1.0 V, the splitting of Mn 3s peak ($\Delta E_s = 5.1$ eV) becomes wider when the valence of Mn in the oxide decreases because of fewer unpaired electrons in the 3d level. Recharging to 1.8 V, the splitting of Mn 3s peak ($\Delta E_s = 4.62$ eV) becomes narrower when the valence of Mn in the oxide increases.

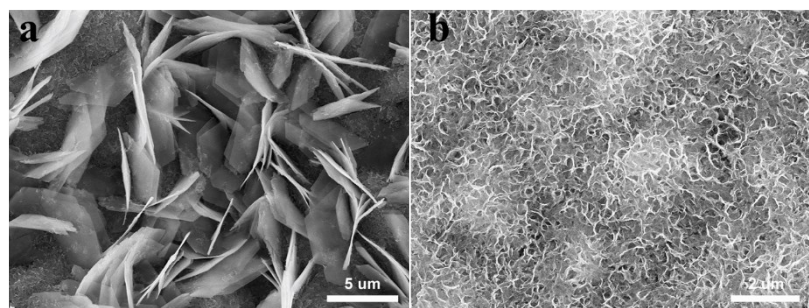


Fig. S20 SEM images of the $\text{MnO}_2@50\text{GDYO}$ cathodes after 1000 cycles (a) discharge state, (b) charge state.

References

- 1 J. J. Wang, J. G. Wang, X. P. Qin, Y. Wang, Z. Y. You, H. Y. Liu and M. H. Shao, Superfine MnO₂ nanowires with rich defects toward boosted zinc ion storage performance, *ACS Appl. Mater. Interfaces*, 2020, **12**, 34949-34958.
- 2 Y. Zhang, S. J. Deng, Y. H. Li, B. Liu, G. X. Pan, Q. Liu, X. L. Wang, X. H. Xia and J. P. Tu, Anchoring MnO₂ on nitrogen-doped porous carbon nanosheets as flexible arrays cathodes for advanced rechargeable Zn-MnO₂ batteries, *Energy Storage Mater.*, 2020, **29**, 52-59.
- 3 Y. Huang, Z. X. Li, S. Y. Jin, S. D. Zhang, H. L. Wang, P. Hiralal, Gehan A.J. Amaratunga, and H. Zhou, Carbon nanohorns/nanotubes: An effective binary conductive additive in the cathode of high energy-density zinc-ion rechargeable batteries, *Carbon*, 2020, **167**, 431-438.
- 4 J. J. Wang, J. G. Wang, H. Y. Liu, Z. Y. You, Z. Li, F. Y. Kang and B. Q. Wei, A highly flexible and lightweight MnO₂/Graphene membrane for superior zinc-ion batteries, *Adv. Funct. Mater.*, 2020, **31**, 2007397.
- 5 N. Palaniyandy, M. A. Kebede, K. Raju, K. I. Ozoemena, L. le Roux, M. K. Mathe and R. Jayaprakasam, α -MnO₂ nanorod/onion-like carbon composite cathode material for aqueous zinc-ion battery, *Mater. Chem. Phys.*, 2019, **230**, 258-266.
- 6 J. J. Wang, J. G. Wang, H. Y. Liu, C. G. Wei and F. Y. Kang, Zinc ion stabilized MnO₂ nanospheres for high capacity and long lifespan aqueous zinc-ion batteries, *J. Mater. Chem. A*, 2019, **7**, 13727-13735.
- 7 M. Q. Liu, Q. H. Zhao, H. Liu, J. L. Yang, X. Chen, L. Y. Yang, Y. H. Cui, W. Y. Huang, W. G. Zhao, A. Y. Song, Y. T. Wang, S. X. Ding, Y. L. Song, G. Y. Qian, H. B. Chen and F. Pan, Tuning phase evolution of β -MnO₂ during microwave hydrothermal synthesis for high-performance aqueous Zn ion battery, *Nano Energy*, 2019, **64**, 103942.
- 8 C. Y. Wang, M. Q. Wang, Z. C. He, L. Liu and Y. D. Huang, Rechargeable aqueous zinc-manganese dioxide/graphene batteries with high rate capability and large capacity, *ACS Appl. Energy Mater.*, 2020, **3**, 1742-1748.
- 9 X. T. Zhang, J. X. Li, H. S. Ao, D. Y. Liu, L. Shi, C. M. Wang, Y. C. Zhu and Y. T.

- Qian, Appropriately hydrophilic/hydrophobic cathode enables high-performance aqueous zinc-ion batteries, *Energy Storage Mater.*, 2020, **30**, 337-345.
- 10 N. Li, G. Q. Li, C. J. Li, H. C. Yang, G. W. Qin, X. D. Sun, F. Li and H. M. Cheng, Bi-cation electrolyte for a 1.7 V aqueous Zn ion battery, *ACS Appl. Mater. Interfaces*, 2020, **12**, 13790-13796.
- 11 Y. D. Jiao, L. Q. Kang, J. B. Gair, K. McColl, J. W. Li, H. B. Dong, H. Jiang, R. Wang, F. Corà, D. J. L. Brett, G. J. He and I. P. Parkin, Enabling stable MnO₂ matrix for aqueous zinc-ion battery cathodes, *J. Mater. Chem. A*, 2020, **8**, 22075-22082.
- 12 X. Gao, H. W. Wu, W. J. Li, Y. Tian, Y. Zhang, H. Wu, L. Yang, G. Q. Zou, H. S. Hou and X. B. Ji, H⁺ -insertion boosted alpha-MnO₂ for an aqueous Zn-ion battery, *Small*, 2020, **16**, 1905842.